How to cite: *Angew. Chem. Int. Ed.* **2022,** *61,* e202212689
International Edition: doi.org/10.1002/anie.202212689
German Edition: doi.org/10.1002/ange.202212689

Anticancer Metallodrug

Organogold(III) Complexes Display Conditional Photoactivities: Evolving From Photodynamic into Photoactivated Chemotherapy in Response to O_2 Consumption for Robust Cancer Therapy

*Yunli Luo, Bei Cao, Mingjie Zhong, Moyi Liu, Xiaolin Xiong, and Taotao Zou**

Abstract: Photodynamic therapy (PDT) is a spatiotemporally controllable, powerful approach in combating cancers but suffers from low activity under hypoxia, whereas photoactivated chemotherapy (PACT) operates in an O_2-independent manner but compromises the ability to harness O_2 for potent photosensitization. Herein we report that cyclometalated gold(III)-alkyne complexes display a PDT-to-PACT evolving photoactivity for efficient cancer treatment. On the one hand, the gold(III) complexes can act as dual photosensitizers and substrates, leading to conditional PDT activity in oxygenated condition that progresses to highly efficient PACT (ϕ up to 0.63) when O_2 is depleted in solution and under cellular environment. On the other hand, the conditional PDT-to-PACT reactivity can be triggered by external photosensitizers in a similar manner in vitro and in vivo, giving additional tumor-selectivity and/or deep tissue penetration by red-light irradiation that leads to robust anticancer efficacy.

Introduction

Photodynamic therapy (PDT) is a clinically-approved, highly-robust form of cancer therapy with numerous advantages over conventional therapy, including noninvasive nature, high tumor selectivity, low drug resistance and lack of side effects.[1] PDT is based on photocatalytic oxidation reactions through photosensitizers to convert tissue O_2 into highly reactive oxygen species, and its therapeutic efficacy is consequently largely depending on local concentration and diffusion of oxygen.[2] However, the oxygen content in solid tumor tissues is low in 0.02–2 %, which is far below normal tissues of 2–9 % O_2, leading to unsatisfactory activity in solid tumors.[3] In addition, consumption of O_2 during PDT may further aggravate tumor hypoxic level, which can promote tumor proliferation, metastasis, and invasion resulting in poor prognosis of treatment.[4] In this regard, designing O_2-independent photosensitizer or photoactivated chemotherapy (PACT) emerge to be highly attractive.[5]

PACT compounds, in which a biologically active species is caged by a photocleavable bond (such as via metal coordination), is another spatiotemporally controllable, tumor-selective therapeutic approach with little reliance on oxygen.[6] In past years, a growing number of metal-based PACT complexes have been developed with notable examples of Pt^{IV}- and Ru^{II}-based prodrugs that can be either photochemically or photocatalytically activated to release bioactive ligands and/or open active metal binding site to elicit potent anticancer activities.[7] Nevertheless, despite being highly promising, PACT complexes lose the robust O_2 photosensitizing capability (in terms of e.g., photoactivation quantum yield and control of drug resistance). In this regard, PACT complexes with additional PDT activity are considered capable of boosting the phototherapeutic efficacy.[8] However, for a PDT process, PACT is a side reaction that will decrease the photosensitizing capacity; and for a PACT compound, PDT will compromise the photoactivating efficiency by competitively quenching the excited state as well. It is of great challenge to address the dilemma allowing a synergistic PDT and PACT process for effective tumor phototherapy.

In the literature, it is known that while many photocatalytic reactions (e.g., redox reactions) can efficiently happen under inert N_2 or Ar atmosphere, their reactivities decreased heavily if opening to air due to the strong quenching effects by O_2 on the triplet excited states of photosensitizers.[9] It is thus possible to harness photocatalytic reactions to maximize the phototherapeutic potency by conditionally sensitizing O_2 under aerated conditions while photocatalytically triggering the PACT process when O_2 is depleted. Based on our previous studies on gold-based anticancer complexes, we considered that gold complexes could be a good starting point for testing the idea: the gold(III) complexes can act as substrates (prodrugs) for photocatalytic activation by generating potent anticancer gold(I) compounds;[10] meanwhile the photosensitizer for triggering such a photocatalytic activation may come from the same gold(III) complex or by external photosensitizers.[10t,11]

Herein we report a PDT-to-PACT evolving photoreactivities of cyclometallated gold(III) complexes respond-

[*] Y. Luo, M. Zhong, M. Liu, Dr. X. Xiong, Prof. Dr. T. Zou
Guangdong Key Laboratory of Chiral Molecule and Drug Discovery, School of Pharmaceutical Sciences, Sun Yat-Sen University
Guangzhou 510006 (P. R. China)
E-mail: zoutt3@mail.sysu.edu.cn
Dr. B. Cao
Warshel Institute for Computational Biology, and General Education Division, The Chinese University of Hong Kong
Shenzhen 518172 (P. R. China)

ing to progressive tumor O_2 consumption. On the one hand, the complex displays a long-lived excited state with lifetime over 100 μs, rendering the complex to be a robust photosensitizer (PDT agent) under aerated condition. In the meantime, its excited state could be quenched by physiological thiols in a weaker but still strong extent, leading to extremely efficient photo-reduction to release bioactive Au^I species with unprecedently high quantum yield ($\phi = 0.63$) under anaerobic condition. As a result, the gold(III) complexes display potent anti-cancer activities under both normoxic 2D monolayer cells and hypoxic 3D tumor spheroids. Of note, such a conditional reactivity could be photocatalytically triggered by external photosensitizers including riboflavin and protoporphyrin in vitro and in vivo, giving further improvement on tumor specificity and/or light penetration depth. To the best of our knowledge, it is the first time that a PDT-to-PACT evolving strategy is developed to enable a very robust cancer therapeutic efficacy.

Results and Discussion

Synthesis, Characterization and Stability of the Gold(III) Complexes

The cyclometalated gold(III)-alkyne complexes containing different types of bidentate CN ligands were prepared similar to the literature procedure (**1a–c**, Figure 1a; **2–4**, Figure S1). All the complexes were characterized by ^1H, ^{13}C and/or ^{19}F NMR, mass spectrometry and elemental analysis (Figure S2–S6, see the Supporting Information). The ^1H-^1H COSY, ^1H-^{13}C HSQC and ^1H-^{13}C HMBC NMR spectra of **1a** are also shown in Figure S2b–d. These complexes are

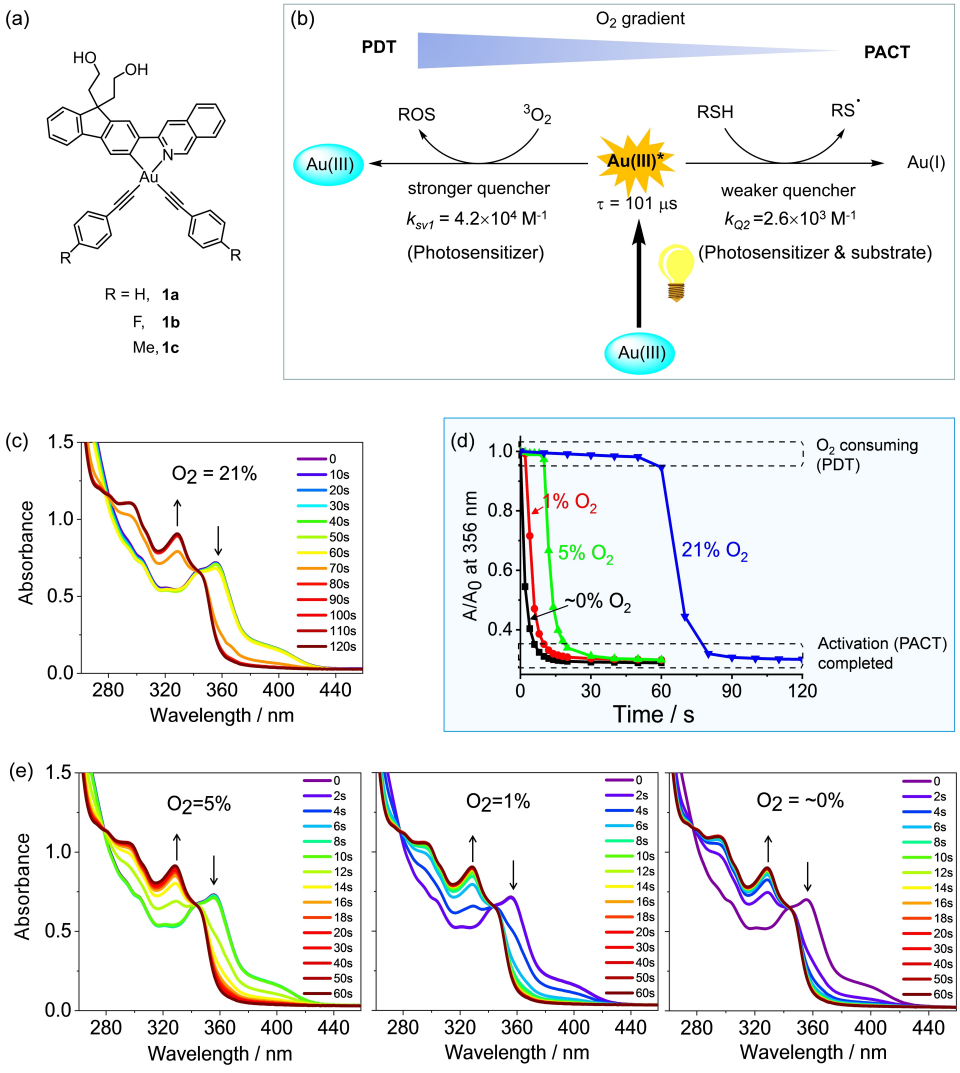

Figure 1. An evolving photo-reactivity in response to progressive oxygen consumption: a) Chemical structures of the gold(III) complexes **1a–c**. b) A graphic description for the PDT-to-PACT evolving process where the gold(III) complex conditionally acts as a PDT agent under oxygenated environment and progresses to photoreduction under hypoxia. c) UV/Vis absorption of **1a** in the presence of NAC in DMSO under 420 nm light irradiation under air. d) Plot of A/A_0 at 356 nm under different O_2 conditions. e) UV/Vis absorption spectra of **1a** with NAC in DMSO under 420 nm light irradiation for different periods at O_2 content of 5%, 1% and 0% (by liquid nitrogen freeze-thawing for three times).

highly soluble in common organic solvents such as DMSO, DMF, $CHCl_3$, CH_3CN and MeOH. Complex **1a–c** and **4** containing two hydroxyl group are soluble in aqueous solution after dilution from the 10 mM DMSO stock solutions.

The stabilities of these gold(III) complexes towards biorelevant thiols were studied by HPLC and UV/Vis absorption experiments. The gold(III) complexes (20 μM) were incubated with 100 equiv of N-acetyl cysteine (NAC) in DMSO and their UV/Vis absorption spectra were monitored (Figure S7a–f). Results showed that **2** (with 2-phenylpyridine as CN ligand) slowly reacted with NAC giving 27 % conversion after 24 h incubation. Increasing the π-conjugation of CN ligand improved the stability (Figure S7a–f, with stability of **1**>**4**>**3**>**2**) and finally **1a** containing fluorene-isoquinoline (FIQ) type CN ligand showed a high stability with no detectable change of UV/Vis absorption after 24 h incubation with NAC. By using HPLC analysis, there was also no change in the LC chromatograms after incubating **1a** with 100-fold NAC for 24 h (Figure S8). Next, the stability of **1a** under cellular conditions was investigated. Melanoma A375 cells were treated with 50 μM of **1a** for 24 h in dark, and then the medium was aspirated and the cells were washed three times with ice-cold PBS followed by cell lysing. HPLC analysis showed that there was a high content of intact **1a** in the supernatant of cell lysate after acetone precipitation with no new peaks in the LC chromatograms (Figure S9). Thus, **1a** has a good stability against biorelevant thiols in solution and in living cells. Complexes **1b** and **1c** displayed a similar stability (Figure S7b, c).

The Oxygen-Dependent Photo-Reactivities in Solution

Afterwards, we examined the photo-reactivity of **1a**. The solution of **1a** (20 μM) with NAC (2 mM) in aerated DMSO was irradiated by 11.1 $mW\,cm^{-2}$ of 420 nm light, and its UV/Vis absorption spectra were recorded (Figure 1c). Interestingly, the absorption of **1a** showed neglected change (<10 % decrease at OD_{356} nm) in the initial 60 s, but the spectra dramatically changed in the next 10 s showing decrease of intensity at 343–450 nm and increase at 300–343 nm, and the reaction started to level off since 80 s (Figure 1c, d). When performing the same experiment in DMF, the absorption spectra remained almost unchanged in a much longer 10 min and then rapidly vanished at ≈350 to 450 nm within 1 min (Figure S10a). In the literature, DMSO, rather than DMF, is known to be a good reductant that can deplete O_2 in the presence of photo-irradiated triplet emitters.[12] Thus, we considered that the different time to rapid change of UV/Vis absorption in DMSO and DMF may be caused by their different O_2 depletion rate. To prove this hypothesis, we conducted UV/Vis absorption of **1a** with NAC in DMSO under different O_2 contents. As shown in Figure 1e, the rapid change of UV/Vis absorption started at 10 s, 2 s and 0 s at 5 %, 1 % and ≈0 % O_2 atmosphere, respectively, all followed by a rapid vanishment of absorbance ($OD_{356\ nm}$) in ≈10 s. Similar trend was again found in DMF under different O_2 contents (Figure S10b–f). By ^1H NMR, the oxidized product dimethylsulfone was detected in the ^1H NMR of **1a** in d_6-DMSO since 5 min of 420 nm light irradiation under air (Figure S11). Thus, the stationary stage during the initial photoirradiation could be attributed to the O_2 consuming process. For **1a** in either degassed or aerated DMSO but without NAC, no obvious reaction was found after 420 nm light irradiation for >5 min (Figure S12). These experiments indicated that **1a** induced an O_2-depletion process in the beginning and progressed to a rapid photoreaction but requiring the participation of thiols (Figure 1b).

To understand such a photo-reactivity, the photophysical and photochemical properties of the gold(III) complex were measured. Complex **1a** showed vibronic emission peaked at 545 nm, which is typical of the metal-perturbed triplet intraligand charge transfer (^{3}ILCT) excited state of the cyclometallated gold(III) complex.[13] Notably, the excited state lifetime was determined to be up to 101 μs in toluene (Figure S13), which led to a strong and dose-dependent quenching effects by O_2 (Figure S14a). The Stern–Volmer quenching constant by O_2 (K_{SV1}) was determined to be as high as $4.23\times10^4\ M^{-1}$. For comparison, the quenching constant by thiols (e.g., 4-chlorothiophenol) is one magnitude weaker with $K_{sv2}=2.62\times10^3\ M^{-1}$ (Figure S14b). The strong quenching effects by O_2 over thiol may account for the two distinct stages, which started from PDT by consuming O_2 and then switched to the rapid photochemical reaction once O_2 was depleted.

Based on the fast UV/Vis response of **1a** with NAC under O_2-depleted conditions (Figure 1e), the quantum yield for the photochemical reaction was estimated following a reported procedure (Figure S15),[14] which was determined to be surprisingly high with $\phi=0.63$, suggesting a super-efficient PACT process.[14] To study the details of photoreaction, the reaction products were examined by HPLC (Figure 2b). Consistent with UV/Vis absorption experiments, **1a** (retention time of 23.2 min) quickly reacted with NAC within 2 min, forming two distinct species in the LC chromatogram with retention time of 13.8 min and 14.1 min, respectively (Figure 2b), which were identified to be phenylacetylene to NAC adduct (PA-NAC) and the CN (FIQ) ligand. By using **1b**, ^1H NMR again showed release of free FIQ ligand after 420 nm photoirradiation in the presence of 100 equiv of NAC in 5 min (Figure S16); in the meantime, the products of PA-NAC and Au^I to PA/NAC adducts were observed in ^1H and ^{19}F NMR (Figure S17). Formation of these products has also been detected by ESI-MS (Figure S18). Thus, **1a** was photochemically reduced by NAC, which released FIQ ligand and formed the reductive elimination product PA-NAC in association with thiol-reactive Au^I species.

To elaborate the mechanism of photoreduction reaction, the following experiments were performed. The reduction potential of the excited state of **1a** [Au^{III}*]/[Au^{II}] was calculated to be +2.23 V based on cyclic voltammetry ([Au^{III}]/[Au^{II}] = −0.65 V, vs SHE, Figure S19a) and UV/Vis absorption ([Au^{III}*]/[Au^{III}] = 2.88 V, Figure 1c). Thus, thiols (([R–S$^\bullet$]/[R–SH] = −80 mV, vs SHE)[10t] can efficiently reduce the photoexcited **1a** via single electron transfer (SET)

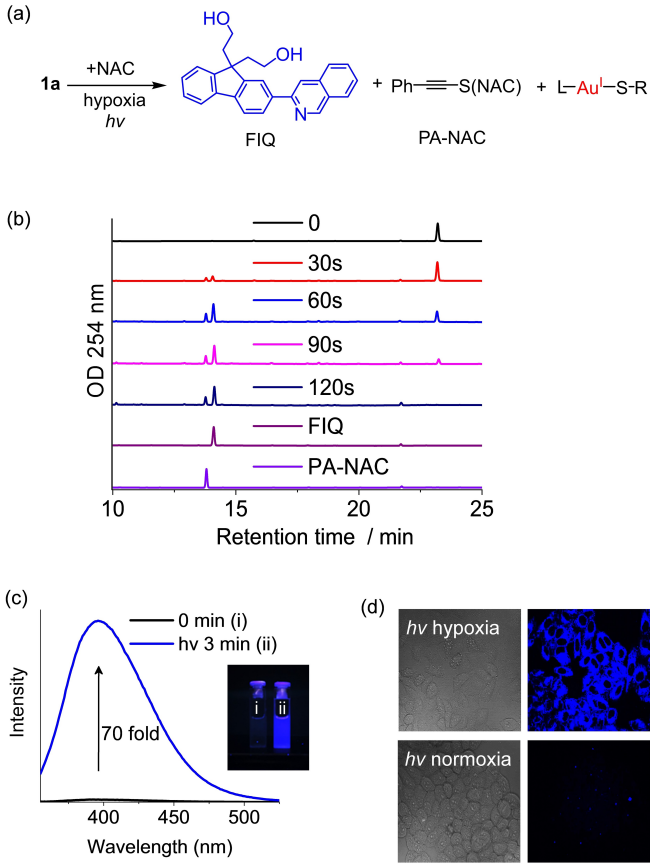

Figure 2. a) Photochemical reaction of **1a** with NAC under light irradiation under hypoxia. b) HPLC analysis for the photoreaction of **1a** with NAC after 420 nm light irradiation for different time in DMSO. c) Emission intensity of **1a** and **1a** after 420 nm photoirradiation for 3 min in DMSO. d) Photoirradiation of **1a** under hypoxia turned on the blue fluorescence in A375 cells.

to generate [Au^{II}]. Based on density functional theory (DFT) calculation, the reduced species from **1a** displayed a distorted geometry with a significant elongated Au-N bond ($\Delta = +0.29$ Å) over other bonds (Figure S20a), indicative of possible breakage at this site. In this regard, the R–S$^{\bullet}$ radical, generated from SET, may directly recombine with Au^{II} radical center (Figure S20a inset) by breaking the Au–N bond, followed by reductive elimination to form PA-NAC adduct and the Au^{I} species. The latter complex can further react with excess NAC and release the CN ligand (Figure S20b). Indeed, when the radical scavenger 2,2,6,6-tetramethylpiperidine-1-oxyl (TEMPO, 1 mM, 0.5-fold relative to NAC) was present in the mixture of **1a** and NAC, the photoreduction was suppressed to 65 % conversion (Figure S21).

Subsequently, we investigated whether the PDT/PACT process would take place in living cells. A375 cells were treated with 50 μM of **1a** for 12 h to allow cellular uptake. Then the cells were irradiated with 420 nm for 2.5 min under hypoxic conditions ($O_2 < 0.1$ %). HPLC analysis showed that a majority of **1a** was reduced in association with a significant amount of FIQ ligand in the supernatant of cell lysate after acetone precipitation (Figure S22). In contrast, at the same 2.5 min light irradiation but under normoxia, a significant amount of intact **1a** with minimal FIQ ligand was detected (Figure S22); instead, staining by Singlet Oxygen Sensor Green (SOSG) showed significant formation of ROS under this aerated condition (Figure S23), indicative of a typical PDT process. Thus, the oxygen-dependent PDT/PACT process can indeed happen under cellular conditions.

On the other hand, it is known that the FIQ ligand is highly emissive, the emission of which is, however, fully suppressed in the gold(III) complex.[15] As a result, the photoreduction-triggered release of FIQ ligand is accompanied by >70-fold increase of emission intensity (Figure 2c). Then, we examined the photoactivation in cells by confocal laser scanning microscopy (CLSM). When A375 cells were treated with 20 μM of **1a** and irradiated by 2.5 min of 420 nm irradiation, bright blue emission at cytoplasmic region was detected in hypoxia but not under aerated condition (Figure 2d), which is consistent with the cellular reactivity by HPLC analysis (Figure S24) and is indicative of the photochemical reduction of **1a** under hypoxic tumor cells. In addition, by using A375 3D tumor spheroids that can mimic the hypoxic tumor microenvironment, similar blue fluorescence and released FIQ ligand were detected (Figure S25).

Since photoreduction of **1a** could release thiol-reactive gold(I) species, we tested its ability to inhibit thioredoxin reductase (TrxR), the critical enzyme that regulates the cellular redox homeostasis and is overexpressed in various cancer cells.[16] The effects of **1a** on purified TrxR enzyme were first investigated. The findings showed that although **1a** was not active in the dark ($IC_{50} > 50$ nM), it significantly reduced TrxR activity after photoactivation with an IC_{50} value of 2.40 ± 0.54 nM, which is comparable to the powerful inhibitor auranofin ($IC_{50} = 1.53 \pm 0.39$ nM). Next, its activity on cellular TrxR was examined. A375 cells were incubated with **1a** for 12 h for effective uptake, and then the cells were treated with or without light irradiation for 5 min under hypoxia, followed by a further 30 min incubation to allow binding/inhibition to TrxR. Results (Table S1) showed that while **1a** did not show inhibition at 25 μM in dark, it potently inhibited TrxR with IC_{50} of 3.10 ± 0.62 μM under light. Such a value is comparable to auranofin treatemnt for 30 min incubation ($IC_{50} = 2.97 \pm 0.50$ μM), suggesting that **1a**, after entering cancer cells, can be efficiently activated by light to release active gold for TrxR inhibition under hypoxia. Interestingly, while **1a** did not show notable reduction after 2.5 min photoirradiation under normoxia (Figure S22), it potently inhibited TrxR after a longer 5 min irradiation, with IC_{50} of 3.90 ± 1.09 μM, suggestive of a possible photoreduction to release active Au species after the initial PDT process. Indeed, the protein bound gold contents after precipitating the cell lysates of **1a** treated cells by acetone showed 15.1 ng/10^5 cells after 5 min irradiation under aerated condition that is much higher than the dark condition (2.69 ng/10^5 cells). Then, the cytotoxicity of the gold complex towards four human cancer cell lines (melanoma cancer A375, colon carcinoma HCT116, lung cancer A549 and hepatocellular carcinoma HepG2) was determined by MTT assay (Table 1). In dark conditions, **1a** was

Table 1: Photocytotoxicity of the gold complexes under normoxia and hypoxia conditions.[a]

	1a			Auranofin		
	Dark	Light[b]		Dark	Light[b]	
		Normoxia	Hypoxia		Normoxia	Hypoxia
A375	>100	0.47±0.03	2.07±0.09	0.95±0.35	0.44±0.01	0.99±0.08
HCT116	>100	0.65±0.31	1.85±0.20	0.65±0.09	0.61±0.10	0.70±0.07
A549	>100	1.23±0.08	2.10±0.11	4.14±0.10	4.20±0.20	4.04±0.40
HepG2	>100	0.90±0.27	5.08±0.40	2.23±0.15	1.60±0.11	1.75±0.23

[a] A total 48 h incubation. [b] 420 nm light irradiation for 5 min.

found non-toxic with IC_{50} >100 μM after 48 h incubation to any of the four cancer cell lines. In contrast, after a short 5 min of 420 nm light irradiation, **1a** exhibited potent cytotoxicity with IC_{50} of 0.47–1.23 μM in oxygenated conditions. Importantly, when the cells were subjected to hypoxic condition, **1a** still exhibited a good photocytotoxicity with IC_{50} of 1.85–5.08 μM, which is ≈5-fold weaker than the normoxia condition but is comparable to auranofin (0.95–4.14 μM). Such a difference may be caused by a combined PDT and PACT process under normoxia rather than the single PACT-activated TrxR inhibition in hypoxia. For comparison, the cytotoxicity of auranofin did not show obvious change between normoxia and hypoxia conditions.

Conditional Photo-Reactivities Induced by Other Photosensitizers in vitro and in vivo

Based on mechanism study, the gold(III) complex simultaneously acts as a photosensitizer and a substrate during the photoactivation process (Figure 3a). We considered that such a photocatalysis-like reaction may be triggered by external photosensitizers provided that they can reduce Au^{III} into Au^{II} (i.e., $\varphi < -0.65$ V). For example, riboflavin (Rf, $[Rf]/[Rf^{\bullet -}] = -1.25$ V vs SHE)[17] is an endogenous photosensitizer that has been used as a PDT agent or photocatalyst.[18] Initially, we tested whether **1a** can be activated by Rf in solution. For the mixture of **1a**, Rf (2.5 equiv) and NAC (100 equiv) in aerated DMSO and under 460 nm irradiation, a stationary stage of **1a** was found in the initial 4 min, followed by photochemical reduction (Figure S26a,c); whereas for the same mixture under degassed condition, an instant photoreduction was found as revealed from UV/Vis absorption (Figure S26b,c) and HPLC analysis (Figure S26d), suggestive of the PDT-to-PACT evolving process in response to O_2 consumption. As a control, in the absence of Rf, **1a** with NAC cannot be activated by 460 nm irradiation (Figure S26e).

In the literature, it is known that riboflavin transporters (RFVTs) are overexpressed in various tumor tissues, and particularly, melanoma was found to strongly overexpress RFVT2 and RFVT3 both intracellularly and on the cell membrane.[19] We tested whether the endogenous Rf (or its metabolized flavin cofactors) could activate the cytotoxicity of the gold(III) complex in cancer cells. Results showed that after 460 nm light irradiation for 10 min, **1a** displayed

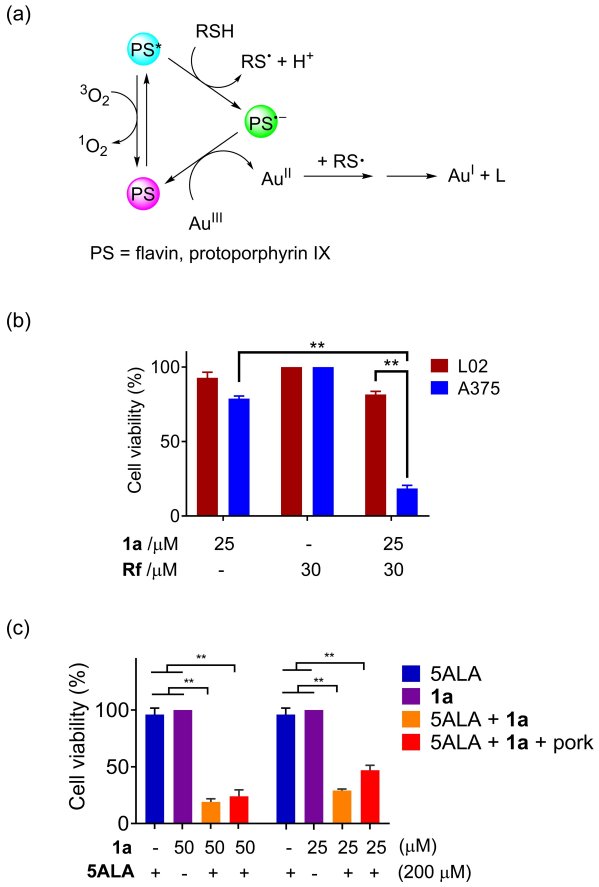

Figure 3. a) Mechanistic description of the PDT-to-PACT evolving process induced by external photosensitizers. b) Selective photocytotoxicity toward cancer (A375) over normal (L02) cells by "**1a**+Rf" after 460 nm photoirradiation under hypoxia. c) Induction of photocytotoxicity by a combination of **1a** and 5ALA by 630 nm red light irradiation with or without a slice of pork.

cytotoxicity IC_{50} of 0.6 μM (A375), 3.0 μM (HepG2), 6.7 μM (A549), and 5.0 μM (HCT116). For comparison, after 420 nm irradiation (under which **1a** could be directly activated), it exhibited very similar cytotoxicity profile to these cell lines (0.47–1.23 μM, Table 1). Thus, the different cytotoxicity under 460 nm irradiation may be attributed to their different cellular flavin levels.[19c,d]

Next, we investigated if **1a** could be activated by 460 nm light in hypoxia. At 25 μM, **1a** moderately inhibited A375

cells with cell viability of 78.8 % whereas it was less photocytotoxic to normal liver cell L02 (viability 92.7 %) under hypoxic conditions. Then, we tested if additionally adding Rf could improve the potency and tumor selectivity. When the cells were co-treated with **1a** (25 μM) and Rf (30 μM), and then the medium was replaced with fresh one followed by 460 nm light irradiation for 5 min under hypoxia, results showed that Rf significantly increased the cytotoxicity of **1a** toward A375 cells with viability of 18.5 %, while the viability of L02 was only slight decreased to 81.5 % (Figure 3b, Rf alone did not cause cytotoxicity under this condition). That is, addition of Rf selectively increased the cytotoxicity towards cancer A375 over normal L02 cells. Such a selectivity has been further confirmed in the A375/L02 co-culture assay by using living/dead cell co-staining assay (Figure S27). Thus, a clear selectivity of "**1a**+Rf" towards cancer cells with high expression of riboflavin transporters was identified.

Afterwards, we investigated if **1a** could be activated by photosensitizers with red absorption. In this regard, we chose clinic protoporphyrin IX (PpIX, $[PpIX]/[PpIX^{\bullet-}] = -1.07$ V vs SHE, Figure S19b) that could be metabolized from 5ALA.[20] After irradiating the equimolar mixture of **1a**, PpIX, and 100 equiv NAC by 630 nm light in degassed DMF, complete reduction of **1a** was found within 30 min based on HPLC analysis (Figure S28). Next, A375 cells were treated with 200 μM of 5ALA for 8 h to allow uptake and PpIX formation; then the cells were treated with **1a** for 4 h followed by aspiration of medium and 630 nm irradiation for 10 min under hypoxia conditions. As depicted in Figure 3c, while single treatment by 5ALA or **1a** did not cause obvious cytotoxicity, the "5ALA+**1a**" combo significantly suppressed cell proliferation with 19 % and 30 % viabilities at 50 μM and 25 μM of **1a**, respectively. Notably, even when the light went through a 6.3 mm slice of pork, such inhibitions were still maintained showing 24 % and 47 % viability, respectively. For comparison, when 420 nm light went through the same pork, no photocytotoxicity was found (Figure S29).

We further evaluated the phototherapeutic activity of the gold(III) complex in vivo. Based on the fact that the thiol-reactive gold(I) complexes can inhibit the blood vessel formation that is associated with tumor angiogenesis,[10e] we studied the activity of "**1a**+5ALA" on blood vessel formation during zebrafish development. The Tg (flk1-EGFP)^{S843} zebrafish embryos were treated with "**1a** (50 μM)+5ALA (500 μM)", or the same concentration of single **1a**, 5ALA, or solvent for 24 h, and then the embryos were subjected to a transient hypoxia environment (<1 % O_2) for 30 min followed by 630 nm light irradiation for 15 min. After a total 3 days of embryo development, the fluorescence images were taken. As shown in Figure 4A, in the group treated by "**1a**+5ALA" by 630 nm irradiation, significant damages of blood vessels, particularly at intersegmental vessel (ISV), dorsal longitudinal anastomotic vessel (DLAV) and caudal vein (CV) were observed, whereas in the group treated by **1a** alone, or 5ALA alone, there were no such damage.

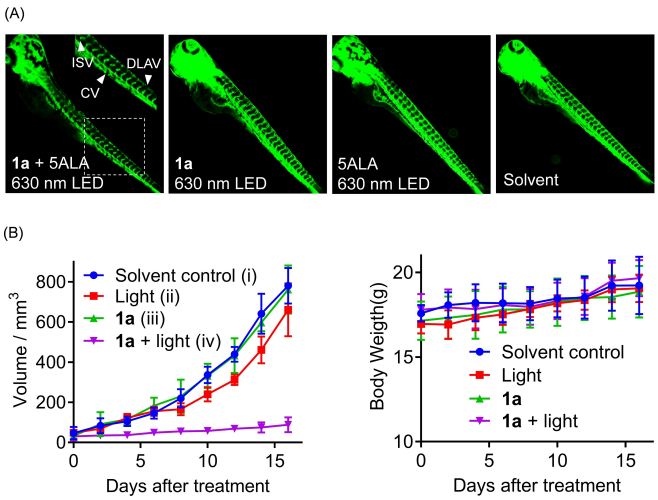

Figure 4. Anti-tumor activities in vivo. A) Fluorescence images of zebrafish (flk-GFP) after treatment of zebrafish embryos by "**1a**+5ALA", **1a**, 5ALA or solvent after 630 nm light irradiation for 15 min under a transient hypoxia condition (<1 % oxygen for 0.5 h). B) The tumor volume (left) and body weight (right) in mice-bearing A375 tumor xenografts after treatment with 3 mg kg^{-1} of **1a** three times per week with or without 465 nm light irradiation.

Next, the anti-tumor activity in mice bearing A375 xenografts were examined by taking advantage of endogenous flavin in melanoma A375 cells. In general, the tumor-bearing mice were injected (i.p.) with 3 mg kg^{-1} of **1a** or solvent once every other day, followed by 465 nm photoirradiation 4 h post injection. As shown in Figure 4B, treatment by **1a** in dark did not cause tumor inhibition compared to the solvent control. For the group treated with light irradiation alone, there was a marginal inhibition on the tumor growth, which is likely caused by the PDT effect of endogenous flavin in A375 tumor but is inefficient due to hypoxic tumor microenvironments. Remarkably, **1a** in 465 nm light irradiation significantly attenuated tumor growth with a 92 % inhibition after 16 days treatment. No mouse death or loss of body weight was found during the treatment (Figure 4B, right). To further examine whether photoreduction of **1a** happened within tumors, the tumors in the "**1a**+light" group at the end of experiment were homogenized and analyzed by HPLC and high-resolution mass spectrometry (Figure S30), the released FIQ ligand was clearly found in the LC chromatogram with *m*/*z* ([FIQ+H], 382.1796) and isotopic pattern matched the simulated values, implying that the gold(III) complex is indeed photocatalytically activatable for tumor inhibition in vivo.

Conclusion

In conclusion, a PDT-to-PACT evolving strategy was, for the first time, identified in cyclometalated gold(III) complexes for tumor phototherapy. On the one hand, the gold(III) complexes can act as dual photosensitizers and substrates, leading to conditional PDT activity in oxy-

genated condition that progresses to highly efficient PACT when O_2 is progressively depleted in solution and under cellular environment. On the other hand, the PDT-to-PACT evolving photo-reactivity can be equally triggered by external photosensitizers which display potent PDT in normoxia and switch to photocatalytic prodrug activation under hypoxia in vitro and in vivo, giving additional tumor-selectivity and deep tissue penetration by red-light irradiation. In view that photocatalysis is potentially capable of activate prodrugs of different complexes (e.g., Pt and Ru) more than Au one, it is envisioned that such a PDT-to-PACT evolving strategy could be extended to develop other metal prodrugs for robust cancer phototherapy.

Experimental Section

The synthesis, characterization, photoreactivities, cellular and animal studies can be found in the Supporting Information.

Acknowledgements

This work was finically supported by National Natural Science Foundation of China (No. 22122706), Guangdong Science and Technology Department (No. 2019QN01C125), Guangdong Basic and Applied Basic Research Foundation (No. 2021A1515012347, 2020A1515110508), Guangzhou Science and Technology Projects (No. 202102020790) and Guangdong Provincial Key Lab of Chiral Molecule and Drug Discovery (No. 2019B030301005). The Warshel Institute for Computational Biology funding from Shenzhen City and Long-gang District is also acknowledged.

Conflict of Interest

The authors declare no conflict of interest.

Data Availability Statement

The data that support the findings of this study are available from the corresponding author upon reasonable request.

Keywords: Anticancer Metallodrug · Gold Medicine · Metal Prodrug · Photoactivated Chemotherapy · Photodynamic Therapy

[1] a) G. Shi, S. Monro, R. Hennigar, J. Colpitts, J. Fong, K. Kasimova, H. Yin, R. DeCoste, C. Spencer, L. Chamberlain, A. Mandel, L. Lilge, S. A. McFarland, *Coord. Chem. Rev.* **2015**, *282–283*, 127–138; b) S. Monro, K. L. Colon, H. Yin, J. Roque III, P. Konda, S. Gujar, R. P. Thummel, L. Lilge, C. G. Cameron, S. A. McFarland, *Chem. Rev.* **2019**, *119*, 797–828; c) H. Shi, P. J. Sadler, *Br. J. Cancer* **2020**, *123*, 871–873; d) P. C. Lo, M. S. Rodriguez-Morgade, R. K. Pandey, D. K. P. Ng, T. Torres, F. Dumoulin, *Chem. Soc. Rev.* **2020**, *49*, 1041–1056; e) J. Karges, *Angew. Chem. Int. Ed.* **2022**, *61*, e202112236; *Angew. Chem.* **2022**, *134*, e202112236; f) K. A. Ryu, C. M. Kaszuba, N. B. Bissonnette, R. C. Oslund, O. O. Fadeyi, *Nat. Chem. Rev.* **2021**, *5*, 322–337; g) T. C. Pham, V. N. Nguyen, Y. Choi, S. Lee, J. Yoon, *Chem. Rev.* **2021**, *121*, 13454–13619.

[2] a) Z. Zhou, J. Song, L. Nie, X. Chen, *Chem. Soc. Rev.* **2016**, *45*, 6597–6626; b) F. Heinemann, J. Karges, G. Gasser, *Acc. Chem. Res.* **2017**, *50*, 2727–2736; c) J. Xie, Y. Wang, W. Choi, P. Jangili, Y. Ge, Y. Xu, J. Kang, L. Liu, B. Zhang, Z. Xie, J. He, N. Xie, G. Nie, H. Zhang, J. S. Kim, *Chem. Soc. Rev.* **2021**, *50*, 9152–9201; d) X. Zhao, J. Liu, J. Fan, H. Chao, X. Peng, *Chem. Soc. Rev.* **2021**, *50*, 4185–4219.

[3] a) J. M. Brown, W. R. Wilson, *Nat. Rev. Cancer* **2004**, *4*, 437–447; b) W. Zeng, P. Liu, W. Pan, S. R. Singh, Y. Wei, *Cancer Lett.* **2015**, *356*, 263–267.

[4] F. Wei, T. W. Rees, X. Liao, L. Ji, H. Chao, *Coord. Chem. Rev.* **2021**, *432*, 213714.

[5] a) H. Huang, S. Banerjee, K. Qiu, P. Zhang, O. Blacque, T. Malcomson, M. J. Paterson, G. J. Clarkson, M. Staniforth, V. G. Stavros, G. Gasser, H. Chao, P. J. Sadler, *Nat. Chem.* **2019**, *11*, 1041–1048; b) J. Du, T. Shi, S. Long, P. Chen, W. Sun, J. Fan, X. Peng, *Coord. Chem. Rev.* **2021**, *427*, 213604; c) L. Huang, S. Zhao, J. Wu, L. Yu, N. Singh, K. Yang, M. Lan, P. Wang, J. S. Kim, *Coord. Chem. Rev.* **2021**, *438*, 213888; d) L. Gourdon, K. Cariou, G. Gasser, *Chem. Soc. Rev.* **2022**, *51*, 1167–1195.

[6] a) N. J. Farrer, L. Salassa, P. J. Sadler, *Dalton Trans.* **2009**, 10690–10701; b) X. Wang, X. Wang, S. Jin, N. Muhammad, Z. Guo, *Chem. Rev.* **2019**, *119*, 1138–1192; c) S. Bonnet, *Dalton Trans.* **2018**, *47*, 10330–10343; d) C. Imberti, P. Zhang, H. Huang, P. J. Sadler, *Angew. Chem. Int. Ed.* **2020**, *59*, 61–73; *Angew. Chem.* **2020**, *132*, 61–73; e) R. Weinstain, T. Slanina, D. Kand, P. Klán, *Chem. Rev.* **2020**, *120*, 13135–13272; f) M. Martínez-Alonso, G. Gasser, *Coord. Chem. Rev.* **2021**, *434*, 213736.

[7] a) F. S. Mackay, J. A. Woods, H. Moseley, J. Ferguson, A. Dawson, S. Parsons, P. J. Sadler, *Chem. Eur. J.* **2006**, *12*, 3155–3161; b) N. J. Farrer, J. A. Woods, L. Salassa, Y. Zhao, K. S. Robinson, G. Clarkson, F. S. Mackay, P. J. Sadler, *Angew. Chem. Int. Ed.* **2010**, *49*, 8905–8908; *Angew. Chem.* **2010**, *122*, 9089–9092; c) F. Barragán, P. Lopez-Senin, L. Salassa, S. Betanzos-Lara, A. Habtemariam, V. Moreno, P. J. Sadler, V. Marchan, *J. Am. Chem. Soc.* **2011**, *133*, 14098–14108; d) B. S. Howerton, D. K. Heidary, E. C. Glazer, *J. Am. Chem. Soc.* **2012**, *134*, 8324–8327; e) M. A. Sgambellone, A. David, R. N. Garner, K. R. Dunbar, C. Turro, *J. Am. Chem. Soc.* **2013**, *135*, 11274–11282; f) T. Joshi, V. Pierroz, C. Mari, L. Gemperle, S. Ferrari, G. Gasser, *Angew. Chem. Int. Ed.* **2014**, *53*, 2960–2963; *Angew. Chem.* **2014**, *126*, 3004–3007; g) B. A. Albani, B. Peña, N. A. Leed, N. A. B. G. de Paula, C. Pavani, M. S. Baptista, K. R. Dunbar, C. Turro, *J. Am. Chem. Soc.* **2014**, *136*, 17095–17101; h) L. N. Lameijer, D. Ernst, S. L. Hopkins, M. S. Meijer, S. H. C. Askes, S. E. Le Dévédec, S. Bonnet, *Angew. Chem. Int. Ed.* **2017**, *56*, 11549–11553; *Angew. Chem.* **2017**, *129*, 11707–11711; i) K. Arora, M. Herroon, M. H. Al-Afyouni, N. P. Toupin, T. N. Rohrabaugh, L. M. Loftus, I. Podgorski, C. Turro, J. J. Kodanko, *J. Am. Chem. Soc.* **2018**, *140*, 14367–14380; j) S. Alonso-de Castro, A. L. Cortajarena, F. López-Gallego, L. Salassa, *Angew. Chem. Int. Ed.* **2018**, *57*, 3143–3147; *Angew. Chem.* **2018**, *130*, 3197–3201; k) Z. Wang, N. Wang, S.-C. Cheng, K. Xu, Z. Deng, S. Chen, Z. Xu, K. Xie, M.-K. Tse, P. Shi, H. Hirao, C.-C. Ko, G. Zhu, *Chem* **2019**, *5*, 3151–3165; l) L. N. Lameijer, C. van de Griend, S. L. Hopkins, A.-G. Volbeda, S. H. C. Askes, M. A. Siegler, S. Bonnet, *J. Am. Chem. Soc.* **2019**, *141*, 352–362; m) V. H. S. van Rixel, V. Ramu, A. B. Auyeung, N. Beztsinna, D. Y. Leger, L. N. Lameijer, S. T. Hilt, S. E. Le Dévédec, T. Yildiz, T. Betancourt, M. B. Gildner, T. W. Hudnall, V. Sol, B. Liagre, A. Kornienko,

S. Bonnet, *J. Am. Chem. Soc.* **2019**, *141*, 18444–18454; n) Z. Deng, N. Wang, Y. Liu, Z. Xu, Z. Wang, T. C. Lau, G. Zhu, *J. Am. Chem. Soc.* **2020**, *142*, 7803–7812; o) J. Karges, T. Yempala, M. Tharaud, D. Gibson, G. Gasser, *Angew. Chem. Int. Ed.* **2020**, *59*, 7069–7075; *Angew. Chem.* **2020**, *132*, 7135–7141; p) G. Thiabaud, R. McCall, G. He, J. F. Arambula, Z. H. Siddik, J. L. Sessler, *Angew. Chem. Int. Ed.* **2016**, *55*, 12626–12631; *Angew. Chem.* **2016**, *128*, 12816–12821.

[8] a) J. D. Knoll, B. A. Albani, C. Turro, *Acc. Chem. Res.* **2015**, *48*, 2280–2287; b) H. D. Cole, J. A. Roque III, G. Shi, L. M. Lifshits, E. Ramasamy, P. C. Barrett, R. O. Hodges, C. G. Cameron, S. A. McFarland, *J. Am. Chem. Soc.* **2022**, *144*, 9543–9547; c) N. Toupin, S. J. Steinke, S. Nadella, A. Li, T. N. Rohrabaugh, E. R. Samuels, C. Turro, I. F. Sevrioukova, J. J. Kodanko, *J. Am. Chem. Soc.* **2021**, *143*, 9191–9205.

[9] D. K. Kölmel, R. P. Loach, T. Knauber, M. E. Flanagan, *ChemMedChem* **2018**, *13*, 2159–2165.

[10] a) W. P. To, K. T. Chan, G. S. Tong, C. Ma, W. M. Kwok, X. Guan, K. H. Low, C. M. Che, *Angew. Chem. Int. Ed.* **2013**, *52*, 6648–6652; *Angew. Chem.* **2013**, *125*, 6780–6784; b) R. Kumar, C. Nevado, *Angew. Chem. Int. Ed.* **2017**, *56*, 1994–2015; *Angew. Chem.* **2017**, *129*, 2024–2046; c) P. J. Barnard, L. E. Wedlock, M. V. Baker, S. J. Berners-Price, D. A. Joyce, B. W. Skelton, J. H. Steer, *Angew. Chem. Int. Ed.* **2006**, *45*, 5966–5970; *Angew. Chem.* **2006**, *118*, 6112–6116; d) I. Ott, *Coord. Chem. Rev.* **2009**, *253*, 1670–1681; e) A. Meyer, C. P. Bagowski, M. Kokoschka, M. Stefanopoulou, H. Alborzinia, S. Can, D. H. Vlecken, W. S. Sheldrick, S. Wölfl, I. Ott, *Angew. Chem. Int. Ed.* **2012**, *51*, 8895–8899; *Angew. Chem.* **2012**, *124*, 9025–9030; f) S. J. Berners-Price, P. J. Barnard, in *Ligand Design in Medicinal Inorganic Chemistry*, Wiley, Hoboken, **2014**, pp. 227–256; g) T. Zou, C. T. Lum, C. N. Lok, J. J. Zhang, C. M. Che, *Chem. Soc. Rev.* **2015**, *44*, 8786–8801; h) J. Fernández-Gallardo, B. T. Elie, T. Sadhukha, S. Prabha, M. Sanaú, S. A. Rotenberg, J. W. Ramos, M. Contel, *Chem. Sci.* **2015**, *6*, 5269–5283; i) C. Bazzicalupi, M. Ferraroni, F. Papi, L. Massai, B. Bertrand, L. Messori, P. Gratteri, A. Casini, *Angew. Chem. Int. Ed.* **2016**, *55*, 4256–4259; *Angew. Chem.* **2016**, *128*, 4328–4331; j) D. Wragg, A. de Almeida, R. Bonsignore, F. E. Kühn, S. Leoni, A. Casini, *Angew. Chem. Int. Ed.* **2018**, *57*, 14524–14528; *Angew. Chem.* **2018**, *130*, 14732–14736; k) A. Casini, R. W.-Y. Sun, I. Ott, in *Metallo-Drugs: Development and Action of Anticancer Agents* (Eds.: S. Astrid, S. Helmut, F. Eva, K. O. S. Roland), De Gruyter, Berlin, **2018**, pp. 199–218; l) M. Mora, M. C. Gimeno, R. Visbal, *Chem. Soc. Rev.* **2019**, *48*, 447–462; m) C. Zhang, P.-Y. Fortin, G. Barnoin, X. Qin, X. Wang, A. Fernandez Alvarez, C. Bijani, M.-L. Maddelein, C. Hemmert, O. Cuvillier, H. Gornitzka, *Angew. Chem. Int. Ed.* **2020**, *59*, 12062–12068; *Angew. Chem.* **2020**, *132*, 12160–12166; n) M. Fares, X. Wu, D. Ramesh, W. Lewis, P. A. Keller, E. N. W. Howe, R. Pérez-Tomás, P. A. Gale, *Angew. Chem. Int. Ed.* **2020**, *59*, 17614–17621; *Angew. Chem.* **2020**, *132*, 17767–17774; o) J.-J. Zhang, M. A. Abu el Maaty, H. Hoffmeister, C. Schmidt, J. K. Muenzner, R. Schobert, S. Wölfl, I. Ott, *Angew. Chem. Int. Ed.* **2020**, *59*, 16795–16800; *Angew. Chem.* **2020**, *132*, 16940–16945; p) R. P. Herrera, M. C. Gimeno, *Chem. Rev.* **2021**, *121*, 8311–8363; q) T. Gamberi, A. Pratesi, L. Messori, L. Massai, *Coord. Chem. Rev.* **2021**, *438*, 213905; r) X.-Q. Zhou, I. Carbo-Bague, M. A. Siegler, J. Hilgendorf, U. Basu, I. Ott, R. Liu, L. Zhang, V. Ramu, A. P. Ijzerman, S. Bonnet, *JACS Au* **2021**, *1*, 380–395; s) M. V. Babak, K. R. Chong, P. Rapta, M. Zannikou, H. M. Tang, L. Reichert, M. R. Chang, V. Kushnarev, P. Heffeter, S. M. Meier-Menches, Z. C. Lim, J. Y. Yap, A. Casini, I. V. Balyasnikova, W. H. Ang, *Angew. Chem. Int. Ed.* **2021**, *60*, 13405–13413; *Angew. Chem.* **2021**, *133*, 13517–13525; t) J. Jiang, B. Cao, Y. Chen, H. Luo, J. Xue, X. Xiong, T. Zou, *Angew. Chem. Int. Ed.* **2022**, *61*, e202201103; *Angew. Chem.* **2022**, *134*, e202201103.

[11] a) H. Luo, B. Cao, A. S. C. Chan, R. W.-Y. Sun, T. Zou, *Angew. Chem. Int. Ed.* **2020**, *59*, 11046–11052; *Angew. Chem.* **2020**, *132*, 11139–11145; b) L. Rocchigiani, M. Bochmann, *Chem. Rev.* **2021**, *121*, 8364–8451.

[12] S. Wan, W. Lu, *Angew. Chem. Int. Ed.* **2017**, *56*, 1784–1788; *Angew. Chem.* **2017**, *129*, 1810–1814.

[13] a) F. F. Hung, W. P. To, J. J. Zhang, C. Ma, W. Y. Wong, C. M. Che, *Chem. Eur. J.* **2014**, *20*, 8604–8614; b) M.-C. Tang, M.-Y. Chan, V. W.-W. Yam, *Chem. Rev.* **2021**, *121*, 7249–7279.

[14] A. Bahreman, J.-A. Cuello-Garibo, S. Bonnet, *Dalton Trans.* **2014**, *43*, 4494–4505.

[15] T. Zou, C. T. Lum, S. S.-Y. Chui, C.-M. Che, *Angew. Chem. Int. Ed.* **2013**, *52*, 2930–2933; *Angew. Chem.* **2013**, *125*, 3002–3005.

[16] a) S. Urig, K. Fritz-Wolf, R. Réau, C. Herold-Mende, K. Tóth, E. Davioud-Charvet, K. Becker, *Angew. Chem. Int. Ed.* **2006**, *45*, 1881–1886; *Angew. Chem.* **2006**, *118*, 1915–1920; b) S. Ray, R. Mohan, J. K. Singh, M. K. Samantaray, M. M. Shaikh, D. Panda, P. Ghosh, *J. Am. Chem. Soc.* **2007**, *129*, 15042–15053; c) J. L. Hickey, R. A. Ruhayel, P. J. Barnard, M. V. Baker, S. J. Berners-Price, A. Filipovska, *J. Am. Chem. Soc.* **2008**, *130*, 12570–12571; d) A. Bindoli, M. P. Rigobello, G. Scutari, C. Gabbiani, A. Casini, L. Messori, *Coord. Chem. Rev.* **2009**, *253*, 1692–1707; e) A. Casini, L. Messori, *Curr. Top. Med. Chem.* **2011**, *11*, 2647–2660; f) M. Frik, J. Fernández-Gallardo, O. Gonzalo, V. Mangas-Sanjuan, M. González-Alvarez, A. Serrano del Valle, C. Hu, I. González-Alvarez, M. Bermejo, I. Marzo, M. Contel, *J. Med. Chem.* **2015**, *58*, 5825–5841; g) A. Giorgio, A. Merlino, *Coord. Chem. Rev.* **2020**, *407*, 213175.

[17] W. Chen, J.-J. Chen, R. Lu, C. Qian, W.-W. Li, H.-Q. Yu, *Bioelectrochemistry* **2014**, *98*, 103–108.

[18] a) S. Alonso-de Castro, E. Ruggiero, A. Ruiz-de-Angulo, E. Rezabal, J. C. Mareque-Rivas, X. Lopez, F. Lopez-Gallego, L. Salassa, *Chem. Sci.* **2017**, *8*, 4619–4625; b) M.-Y. Yang, C.-J. Chang, L.-Y. Chen, *J. Photochem. Photobiol. B* **2017**, *173*, 325–332; c) J. Gurruchaga-Pereda, V. Martínez-Martínez, E. Rezabal, X. Lopez, C. Garino, F. Mancin, A. L. Cortajarena, L. Salassa, *ACS Catal.* **2020**, *10*, 187–196.

[19] a) A. A. Karande, L. Sridhar, K. S. Gopinath, P. R. Adiga, *Int. J. Cancer* **2001**, *95*, 277–281; b) X. R. Jiang, X. Y. Yu, J. H. Fan, L. Guo, C. Zhu, W. Jiang, S. H. Lu, *Cancer Lett.* **2014**, *353*, 78–86; c) L. Bartmann, D. Schumacher, S. von Stillfried, M. Sternkopf, S. Alampour-Rajabi, M. van Zandvoort, F. Kiessling, Z. Wu, *Front. Pharmacol.* **2019**, *10*, 79; d) M. Darguzyte, N. Drude, T. Lammers, F. Kiessling, *Cancers* **2020**, *12*, 295.

[20] M. Ishizuka, F. Abe, Y. Sano, K. Takahashi, K. Inoue, M. Nakajima, T. Kohda, N. Komatsu, S. Ogura, T. Tanaka, *Int. Immunopharmacol.* **2011**, *11*, 358–365.

Manuscript received: August 28, 2022
Accepted manuscript online: September 15, 2022
Version of record online: October 6, 2022